THE FINITE DIFFERENCE CONTRAST SOURCE INVERSION WITH SUPER MEMORY HYBRID CONJUGATE GRADIENT METHOD

DOUDOU WANG, SHOUDONG WANG and HONGLIANG LI

China University of Petroleum (Beijing), State Key Laboratory of Petroleum Resource and Prospecting; National Engineering Laboratory of Offshore Oil Exploration; CNPC Key Laboratory of Geophysical Exploration, Beijing, P.R.China. ctlab@cup.edu.cn

ABSTRACT

Wang, D.D., Wang, S.D. and Li, H.L., 2020. The finite difference contrast source inversion with super memory hybrid conjugate gradient method. *Journal of Seismic Exploration*, 29: 73-97.

The finite difference contrast source inversion (FDCSI) is an algorithm to solve the wave equation inverse scattering problem. This algorithm's forward operator is only related to the background medium, which does not change during the iterative optimization process. Therefore, an LU decomposition is required only once for the forward operator, which has lower computation cost. Because of finite difference operator, FDCSI can be applied to inhomogeneous background medium. FDCSI transforms the inverse scattering problem of wave equation into an optimization problem, which can be solved by conjugate gradient method. But conventional conjugate gradient method converges slowly, which affects computing efficiency, and the Newton method increases computation and memory. In order to improve the convergence speed for frequency domain acoustic equation, the super memory hybrid conjugate gradient method (SMHCG) is introduced into FDCSI. SMHCG is improved on the basis of the super memory gradient method to adapt to FDCSI. SMHCG accelerates the convergence of objective function without any increase computation and memory. The advantages of SMHCG had been verified on the Marmousi model.

KEYWORDS: contrast source inversion, scattering, super memory hybrid conjugate gradient method, full waveform inversion.

INTRODUCTION

Full waveform inversion is one high-precision reconstruction method for underground complex structure, which makes use of the kinematics and dynamics of seismic wave information and take the seismic wave equation as the carrier to realize the inversion of underground physical parameters, provide migration velocity and it can also be used for the reservoir development. Full waveform inversion can be performed both in the time domain (Tarantola, 1986) and frequency domain (Pratt and Worthington, 1990). Full waveform inversion mainly consists of forward and inversion. Forward can be solved using iterative methods and direct solutions. Inversion is to modify the initial model by iterative optimization to meet the error requirement. Iterative optimization method is the most important part of the full waveform inversion. At present, most full waveform inversion optimization algorithm is divided into two categories. The first category is the gradient method based on the cost function gradient, for example steepest descent method (Choi et al., 2005; Jiang et al., 2009; Chi et al., 2014) and conjugate gradient (Pratt, 1999; Kamei et al., 2014) method. The second category is the Newton optimize methods, such as Gauss Newton method (Pratt et al., 1998), truncated Newton method (Métivier et al., 2014) and Quasi-Newton method (Brossier et al., 2009). Although Newton's method converges faster than the gradient method, more computation and memory are needed. Generally, the inversion process requires huge amount of computation. It is of great significance to reduce the amount of inversion computation in the inversion.

Van den Berg and Kleinman (1997) introduced the contrast source inversion (CSI) method based on inverse scattering theory. This method is based on the improvement of source-type integration method (Habashy et al., 1994), which is a highly efficient nonlinear inversion method. This method updates the contrast source (the multiplication of the model parameters and the wavefield) and the contrast function (model parameters) by optimizing the objective function. In the whole iterative optimization process, this method needs only once full forward, so it can greatly improve the inversion efficiency. Moreover, van den Berg et al. (1999) extended the method to microwave imaging and achieved better results. For the first time, Pelekanos et al. (2003) applied contrast source inversion to elastomechanics imaging and proposed the regularization of multiplication to enhance the stability of the method. Van Dongen and Wright (2007) applied this method to three-dimensional acoustic imaging, and verified the effectiveness of the method. Wang et al. (2016) based on the integral equation (IE) formulation to achieved multi-frequency CSI, and used the WKBJ approximation method to get the Green function. However, the main disadvantage of CSI based on the integral equation (IE) formulation is only applicable to simple medium (homogeneous or layered medium), since the Green function of background medium can be obtained. Considering the limitation of the Green function, Abubakar et al. (2008, 2009) further expand the CSI

algorithm and proposed finite difference contrast source inversion (FDCSI). FDCSI is applied to seismic data inversion. This method is suitable for any background model, greatly broadening the scope of application of contrast source inversion. The forward operator of FDCSI algorithm is only related to the background model and the frequency. In the inversion process, if the background model and the frequency are not changed, there is no need to reconstruct the forward operator. In the single-frequency inversion process, due to the invariant forward operation, LU decomposition is required only once, which greatly improve efficiency. Base on those advantages, FDCSI has the ability to deal with large-scale data (Abubakar et al., 2011). Han et al. (2014, 2016) achieved FDCSI with elastic wave equation and acoustic wave equation, respectively, and achieved multi-parameter inversion.

Although FDCSI algorithm is fast, the conventional conjugate gradient method converges slowly. Newton method can speed up the convergence rate, but it will increase calculation and memory consumption. In this paper, we use super memory hybrid conjugate gradient method (SMHCG) to optimize the cost function based on finite difference contrast source inversion. We obtain super memory hybrid conjugate gradient method (SMHCG) by improving the super memory gradient method (SMG) (Shi and Shen, 2005; Hu et al., 2016; Ou and Liu, 2014, 2017), so that it can adapt to FDCSI. The super memory hybrid conjugate gradient method (SMHCG) is a fast convergence optimization method. Compared with the conventional conjugate gradient method, the SMHCG method has a faster convergence speed. The new gradient is obtained by using the previous update gradient and n-th gradient, which doesn't increase the amount of computation and solves the problem of expensive computation and slow convergence speed well. We have obtained good results by model numerical experiment.

FORWARD MODELING

Forward is the basis of inversion. The two-dimensional frequency domain acoustic equation is described as follows

$$[\nabla^2 + k^2(r)]p(r) = S(r, \omega) \quad , \tag{1}$$

where ∇ is the Laplace operator, r is the space coordinate vector, $k(r)$ is the wave number and $p(r)$ is the wave field value. The wave number $k(r)$ is as follows

$$k(r) = \frac{\omega}{c(r)} \quad , \tag{2}$$

where $c(r)$ is the velocity of model, and ω is the circular frequency.

The frequency seismic numerical simulation method is presented by Lysmer and Drake (1972), which has more advantages than time domain and has been studied by many scholars (Pratt and Worthington, 1990; Shin, 1995; Sirguel and Pratt, 2004). In this paper, the optimal 9-point finite difference (Jo et al., 1996) is used as forward engine. This forward method uses the cartesian coordinates of the grid and the 45° rotating grid, using 9 difference schemes, the method reduces the grid point in each wavelength by five, the coefficient matrices consist of 9 bands. In this paper, in order to simplify the calculation, we assume that the medium model density is uniform.

The model media is divided into N_x x N_z uniform grid region (including PML area) grids. According to the discrete grid, eq. (1) can be sorted into the following matrix form

$$HP = S \quad , \tag{3}$$

where H is the forward operator, P is the value of the wave field which is a one-dimensional vector. The eq. (3) can be solved by LU decomposition (Davis and Duff, 2006) and iterative method. In this paper, we use the LU decomposition method to solve eq. (3), and the results of the LU decomposition can be applied to all sources.

INVERSION METHOD

Problem statement

The contrast source inversion method is used to solve the inverse scattering problem (van den Berg and Kleinman, 1997). For this purpose, we first establish the inverse scattering problem. The two dimensional scattering systerm comprises the object domain D, observation domain S (geophone location) and total domain T, see Fig. 1. The r = (x, y) is the space coordinate vector in R^2. If the parameters in D differ from the parameters of the background model, scattered wave will be generated and received by the detector arranged on the S-field. We use the scattered wave information received by the detector to reconstruct the medium parameters of the D domain.
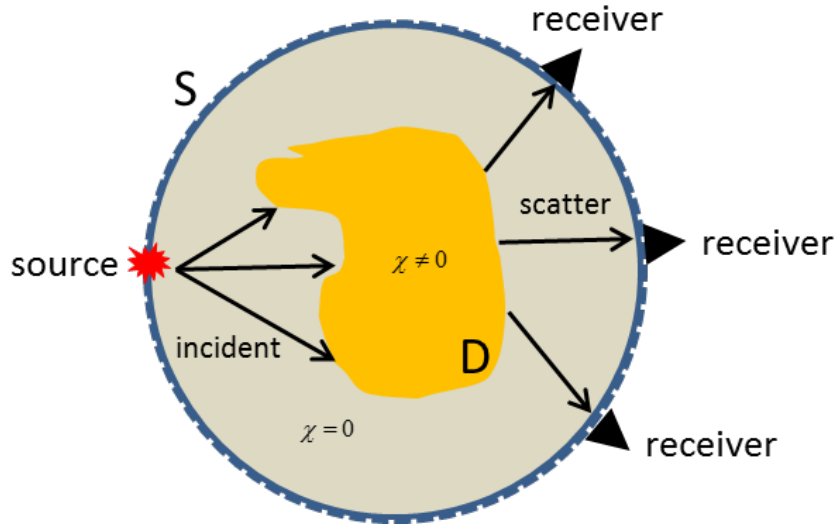
Fig. 1. Schematic of scattering.

For the sake of derivation, all of the following formulas are derived in matrix form.

The total wave fields U^{tol} and incident wave fields U^{inc} satisfy the following two equations in matrix form

$$HU_j^{tol} = S_j, \quad r \in T \tag{4}$$

$$H_b U_j^{inc} = S_j, \quad r \in T \tag{5}$$

where H is the sparse stiffness matrix of the model, H_b is the sparse stiffness matrix of the background model, j is the source number, S_j is the source term.

The contrast function χ is given by

$$\chi(r) = \left[\frac{k(r)}{k_b(r)}\right]^2 - 1 = \frac{c^{-2}(r) - c_b^{-2}(r)}{c_b^{-2}(r)}, \quad r \in D \tag{6}$$

where k and c are wave number and velocity of the model, k_b and c_b are wave number and velocity of the background model.

The scattering wave field is given by

$$U_j^{sct} = U_j^{tol} - U_j^{inc}, \quad r \in T \tag{7}$$

according to the relation of (7), we can get the scattering wave field equation as follows

$$U_j^{sct} = A_b^{-1} \chi U_j^{tol}, \quad r \in T \tag{8}$$

where $A_b = K_b^{-1} H_b$, K_b is the wave number diagonal matrix of the background model, and χ is a diagonal matrix of contrast function.

Because the detector is arranged in the S domain, a mapping relationship is needed to map the scattered wave field to the S domain, so that the data equation can be obtained as follows

$$U_j^{sct} = M^S \left(A_b^{-1} \chi U_j^{tol} \right), \quad r \in S \tag{9}$$

where M^S is an operator that maps the scattering wave field in the T domain to the S domain.

According to eq. (7), we can get the form of the object (or domain) equation of state as follows

$$U_j^{tol} = U_j^{inc} + M^D \left(A_b^{-1} \chi U_j^{tol} \right), \quad r \in D \tag{10}$$

where M^D is an operator that maps the scattering wave field from the T domain to the D domain.

For eq. (10), forward problem is to find U_j^{sct} for given χ, inverse scattering problem is to find χ for given U_j^{sct}.

We define the contrast source (scattered source) as follows

$$W_j = \chi U_j^{tol} \qquad . \tag{11}$$

Then data eq. (9) and object (or domain) eq. (10) are transformed into the following form

$$U_j^{sct} = M^S \left(A_b^{-1} W_j \right), \quad r \in S \tag{12}$$

$$W_j = \chi U_j^{inc} + \chi M^D \left(A_b^{-1} W_j \right), \quad r \in D \qquad . \tag{13}$$

In the actual situation of seismic exploration, T domain and D domain are equal. To simplify the derivation, replace the T domain with the D domain.

The finite difference contrast source inversion method

The FDCSI is a method that does not need to full forward in each inversion iteration (Abubakar et al., 2008, 2009). In the FDCSI method, the inverse scattering problem is considered as an optimization problem. However, FDCSI is different from conventional full wave inversion, it constructs contrast source and contrast function iteratively based on data eq. (12) and object eq. (13). The form of cost function established on the basis of satisfying eqs. (12) and (13) is as follows

$$C(\chi, W_j) = C^S(W_j) + C^D(W_j, \chi)$$

$$= \frac{\sum_j \left\| d_{obs,j}^{sct} - M^S(A_b^{-1} W_j) \right\|_S^2}{\sum_j \left\| d_{obs,j}^{sct} \right\|_S^2} + \lambda \frac{\sum_j \left\| \chi U_j^{inc} - W_j + \chi M^D(A_b^{-1} W_j) \right\|_D^2}{\sum_j \left\| \chi U_j^{inc} \right\|_D^2} \quad , \quad (14)$$

where $C^S(W_j)$ is data errors, $C^D(W_j, \chi)$ is object errors, $d_{obs,j}^{sct}$ is the scattering record received on the surface.

The L2-norm is defined as

$$\|a\|_S^2 = \int_S a(r) \overline{a}(r) dr$$

$$\|a\|_D^2 = \int_D a(r) \overline{a}(r) dr \qquad , \qquad (15)$$

where $\overline{a}(r)$ is the complex conjugate form of $a(r)$.

Define the data errors and object errors in the n-th iteration as follows:

$$\phi_{j,n} = d_{obs,j}^{sct} - M^S(A_b^{-1} W_{j,n})$$

$$\varphi_{j,n} = \chi_n U_j^{inc} - W_{j,n} + \chi_n M^D(A_b^{-1} W_{j,n}) \qquad . \qquad (16)$$

The CSI algorithm is different from the conventional full waveform inversion. The CSI method is divided into two parts, first update the contrast source, and then update the contrast to complete an iterative process.

According to the definition of gradient, the gradient of contrast source W_j can be obtained as follows (Abubakar et al., 2008b)

$$g_{j,n}^W = \frac{\partial C^S(W_j)}{\partial W_j}\bigg|_{W_j = W_{j,n-1}} + \frac{\partial C^D(W_j, \chi_{n-1})}{\partial W_j}\bigg|_{W_j = W_{j,n-1}} \qquad , \qquad (17)$$

$$= -2\eta^S (A_b^*)^{-1} M^{S*} \phi_{j,n-1} - 2\lambda \eta_n^D \left[\varphi_{j,n-1} - (A_b^*)^{-1} M^{D*} (\overline{\chi}_{n-1} \varphi_{j,n-1}) \right]$$

where A_b^*、 M^{S*} and M^{D*} is the conjugate transpose operator (the adjoint operator) of A_b、 M^S and M^D. The normalization factor η^S and η_n^D can be obtained by $\eta^S = \left(\sum_j \left\| d_{obs,j}^{sct} \right\|_S^2 \right)^{-1}$ and $\eta_n^D = \left(\sum_j \left\| \chi_{n-1} U_j^{inc} \right\|_D^2 \right)^{-1}$.

The conventional Polak-Ribière conjugate gradient method is used to update the comparison source, and the search direction is as follows

$$v_{j,0} = 0, \qquad\qquad n = 0$$

$$v_{j,n} = g_{j,n}^W + \frac{\sum_k \left\langle g_{j,n}^W, g_{j,n}^W - g_{j,n-1}^W \right\rangle_D}{\sum_k \left\| g_{j,n-1}^W \right\|_D^2} v_{j,n-1}, \quad n > 0 \qquad (18)$$

The contrast source update formula is given by

$$W_{j,n} = W_{j,n-1} + \alpha_{j,n}^W v_{j,n} \quad, \qquad\qquad (19)$$

where $\alpha_{j,n}^W$ is an update-step.

We assume that the update-step is known, so we can obtain the latest contrast source $W_{j,n}$. The latest contrast source is substituted in eq. (14) to get new equation, then we can obtain the value of update-step by minimizing the new equation. The update-step as follows

$$\alpha_{j,n}^W = \frac{-\sum_j \left\langle g_{j,n}^W, v_{j,n} \right\rangle_D}{\eta^S \sum_j \left\| M^S \left(A_b^{-1} v_{j,n} \right) \right\|_S^2 + \lambda \eta_n^D \sum_j \left\| v_{j,n} - \chi_{n-1} M^D \left(A_b^{-1} v_{j,n} \right) \right\|_D^2} \quad. \quad (20)$$

After obtaining the updated contrast source, the total wave field is updated by (10) and the contrast function is updated by eq. (11). The formula is as follows

$$U_{j,n}^{tol} = U_j^{inc} + M^D (A_b^{-1} W_{j,n}) \quad, \qquad\qquad (21)$$

$$\chi_n = \frac{\sum_j \mathrm{Re}(W_{j,n} \overline{U}_{j,n}^{tol})}{\sum_j \left| U_{j,n}^{tol} \right|^2} \quad. \qquad\qquad (22)$$

The initial model has a great influence on the inversion results. In the case of the known background model, we use the backpropagation field multiplied by a weight coefficient as the initial contrast source. We can also get the corresponding initial contrast function (Abubakar et al., 2009)

$$W_{j,0} = \frac{\left\| \left(A_b^*\right)^{-1} \left(M^{S*}[d_{obs,j}^{sct}]\right) \right\|_D^2}{\left\| M^S \left\{ A_b^{-1} \left[\left(A_b^*\right)^{-1} \left(M^{S*}[d_{obs,j}^{sct}]\right) \right] \right\} \right\|_S^2} \left(A_b^*\right)^{-1} \left(M^{S*}\left[d_{obs,j}^{sct}\right]\right) \tag{23}$$

$$U_{j,0}^{tol} = U_j^{inc} + M^D \left(A_b^{-1} W_{j,0}\right) \tag{24}$$

$$\chi_0 = \frac{\sum_j \mathrm{Re}(W_{j,0}\overline{U}_{j,0}^{tol})}{\sum_j \left|U_{j,0}^{tol}\right|^2} \tag{25}$$

The main computational cost of the whole inversion process is computing operators $\left(A_b\right)^{-1}$ and $\left(A_b^*\right)^{-1}$, which are only related to the background model and the inversion frequency. However, the background model is not updated during the inversion of a single- frequency. Therefore, operators $\left(A_b\right)^{-1}$ and $\left(A_b^*\right)^{-1}$ are invariant during the inversion of a single-frequency. In the single-frequency inversion, we only need to use LU decomposition once to solve the operators $\left(A_b\right)^{-1}$ and $\left(A_b^*\right)^{-1}$, thus greatly improving the computational efficiency and speed.

Although the FDCSI method needs only once full forward and saves the computation time, the conventional Polak-Ribière conjugate gradient method has the problem of slow convergence speed. Newton's method has the advantages of fast convergence but complicated calculation and time-consuming. In this paper, we propose a super memory hybrid conjugate gradient method based on the super memory gradient method, which accelerates the convergence rate.

Super memory hybrid conjugate gradient method

The super memory gradient method (SMG) uses the information of the previous gradient and the current gradient information to reconstruct a new gradient, and the new gradient is used to update the iterative equation (Shi and Shen, 2005; Hu et al., 2016; Ou and Liu, 2014, 2017). Compared with the conventional conjugate gradient method, the SMG can obtain more accurate update information by using more information of the previous gradients. The SMG method is superlinear convergence, so it can accelerate the convergence of objective function. The validity of SMG method has been verified in the conventional full waveform inversion experiment for frequency domain wave equation (Hu et al., 2016). For conventional full waveform inversion, there are two methods to obtain update step length, one is fixed step length, and the other is obtained by linear search method. For the first, the fixed step length of the SMG method has not used the convergence criterion to restrain the cost function, which leads to the

unstable results of the full waveform inversion in the high frequency section. For the second, it can get better results by using the linear search constraint condition to obtain the step length to update the iterative equation.

The SMG method based on linear search constraints can perform better results, but linear search requires huge amount of computation. In the process of contrast source inversion, the update gradient of the contrast source is complex, and there are some problems when using linear search to determine the step length in the complex domain. As a result of the above problems, we improved the super memory gradient method and proposed Super memory hybrid conjugate gradient method (SMHCG) based on the contrast source inversion. The SMHCG method uses the information of the previous update direction and the current gradient information to reconstruct a new gradient, and updating iterative equation by conjugate gradient method. In this way, we can get optimal step length by eq. (20), and avoid linear search. Through numerical experiments, we find that there will be a phenomenon of convergence instability when the cost functional value is too small by iteratively updating. So, by intelligent judgement, when the convergence is unstable, we will use conventional gradient instead of super memory gradient and then construct conjugate gradient, which can effectively solve the phenomenon of inversion instability. In this paper, the contrast source is updated by SMHCG method, and the contrast function is updated by (21) and (22).

The gradient of SMHCG is given by

$$
g_{j,n}^{W\_\mathrm{super}} = \begin{cases} - g_{j,n}^{W} - \sum_{i=2}^{M} \beta_n^i g_{j,n-i}^{W\_\mathrm{super}} & n < N_{unstable} \\ - g_{j,n}^{W} & n \geq N_{unstable} \end{cases} \tag{26}
$$

where $\beta_n^i = -\dfrac{\rho \left\| g_{j,n}^{w} \right\|}{\left\| g_{j,n}^{w\_\mathrm{super}} \right\|}$, $\rho \in \left(0, \dfrac{1}{M} \right)$. M is a positive integer. $N_{unstable}$ is

the number of iterations when there is instability.

The contrast source is updated with a new gradient as follows

$$
v_{j,0}^{\mathrm{super}} = 0, \qquad\qquad n = 0
$$

$$
v_{j,n}^{\mathrm{super}} = g_{j,n}^{W\_\mathrm{super}} + \frac{\sum_k \left\langle g_{j,n}^{W\_\mathrm{super}}, g_{j,n}^{W\_\mathrm{super}} - g_{j,n-1}^{W\_\mathrm{super}} \right\rangle_D}{\sum_k \left\| g_{j,n-1}^{W\_\mathrm{super}} \right\|_D^2} v_{j,n-1}^{\mathrm{super}}, \qquad n > 0 \tag{27}
$$

$$
W_{j,n} = W_{j,n-1} + \alpha_{j,n}^{W\_\mathrm{super}} v_{j,n}^{\mathrm{super}} , \tag{28}
$$

according to the following formula to update the step $\alpha_{j,n}^{W\_\sup er}$:

$$\alpha_{j,n}^{W\_\sup er} = \frac{-\sum_{j}\left\langle g_{j,n}^{W\_\sup er}, v_{j,n}^{\sup er}\right\rangle_{D}}{\eta^{S}\sum_{j}\left\|M^{S}\left(A_{b}^{-1}v_{j,n}^{\sup er}\right)\right\|_{S}^{2} + \lambda\eta_{n}^{D}\sum_{j}\left\|v_{j,n}^{\sup er} - \chi_{n-1}M^{D}\left(A_{b}^{-1}v_{j,n}^{\sup er}\right)\right\|_{D}^{2}} . \quad (29)$$

The SMHCG FDCSI algorithm shown in Fig. 2.
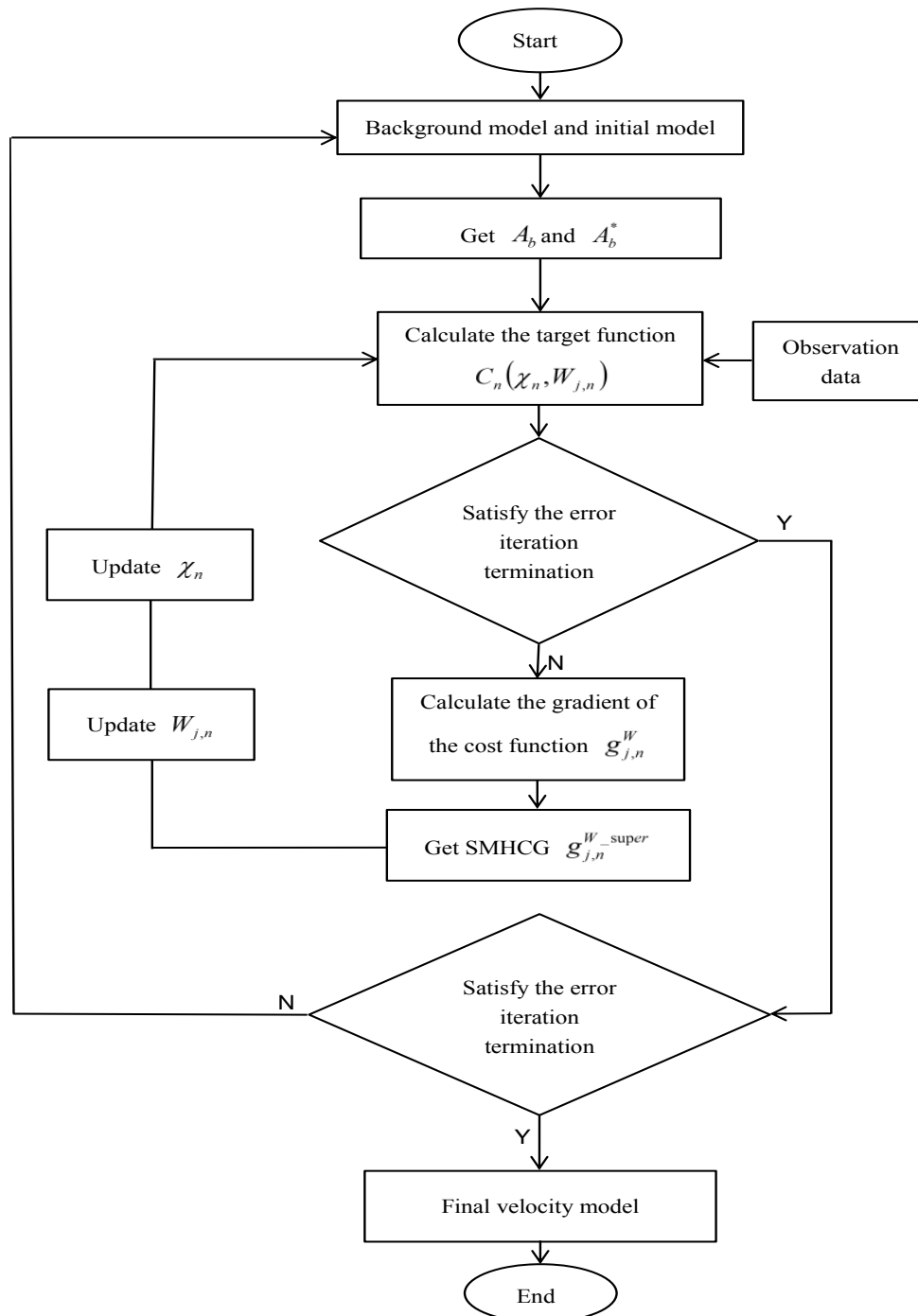
Fig. 2. Algorithm flow diagram.

NUMERICAL EXAMPLES

In order to verify the convergence of SMHCG method, a horizontal layered model and a Marmousi model are used for numerical experiments. In this paper, we choose strategy that the inversion result of the previous frequency is used as the background model for the next frequency inversion. We assume that the density of the model is constant. We use ricker wavelet as source wavelet whose domain frequency is 10 Hz. Fig. 3a shows ricker wavelet in time domain, the domain frequency of ricker wavelet is 10 Hz. Fig. 3b shows spectrum of the ricker wavelet with the domain frequency of 10 Hz. Although the domain frequency of ricker wavelet is 10 Hz, there is a lot of information about ricker wavelet when the frequency component is greater than 10 Hz. So, in horizontal layered model and Marmousi model, we will select some frequencies which is greater than 10 Hz for CSI. We employed PML for contrast source forward and inversion.

(a) (b)
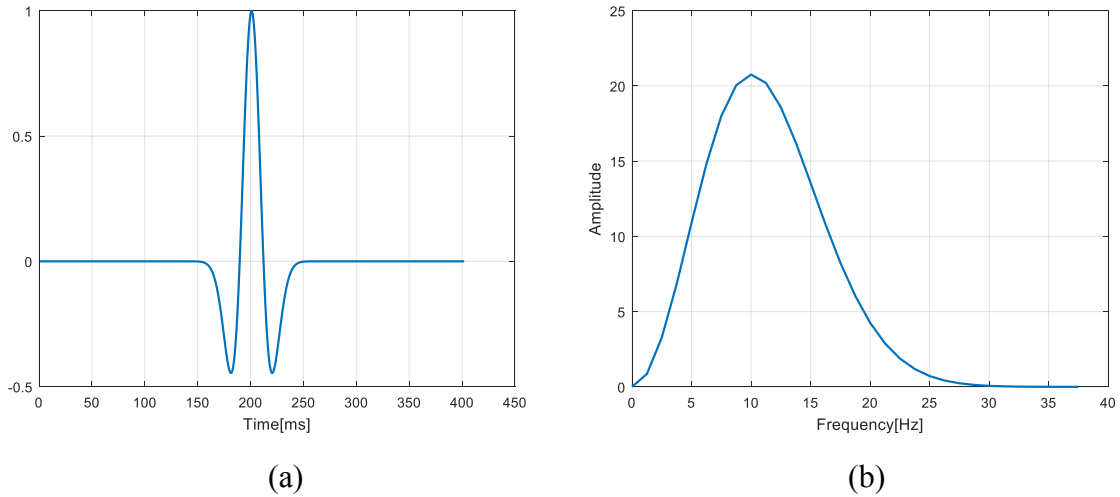
Fig. 3. (a) The Ricker wavelet in time domain, and (b) the spectrum of the Ricker wavelet with the domain fequency of 10 Hz.

Horizontal layered model

A simple layered model is shown in Fig. 4a and the velocity varies from 2000 m/s to 2600 m/s. In the inversion process, the model is 1000m×490m and the spatial grid spacing $\Delta x = \Delta z = 10\,m$. The acquisition system consists of 26 explosive sources and 101 receivers. Each shot sets 101 receivers, and detector spacing of 10 m, shot spacing of 40 m. The detectors are uniformly distributed at z = 20 m. The sources are uniformly distributed at z = 20 m. The initial background model is a linear velocity shown in Fig. 4b. Considering the results of inversion and selection criteria of frequency (Sirgue et al., 2004) we choose 6 frequencies for inversion (3 5 8 12 17 Hz) with 40 iterations per frequency. Memory M = 6, weight factor $\lambda = 1.2$.
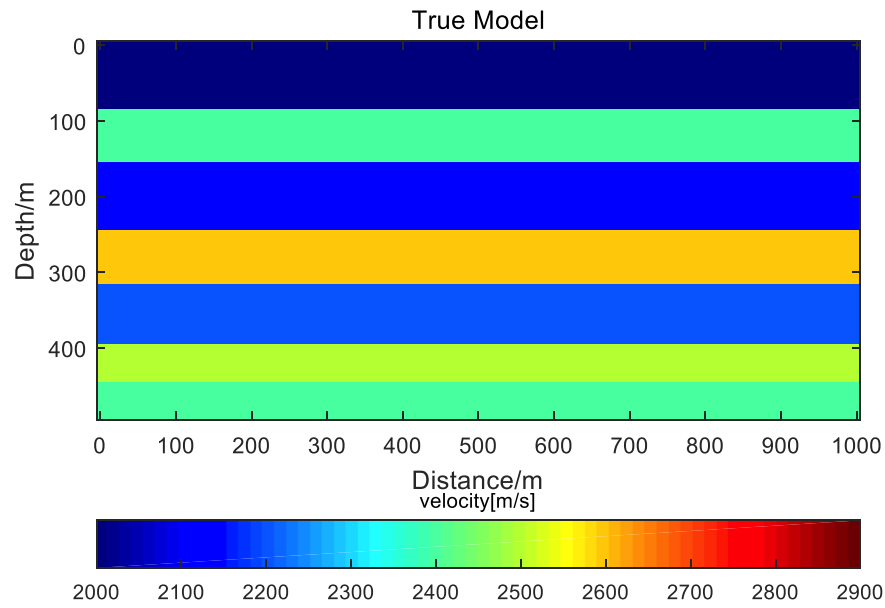
(a)
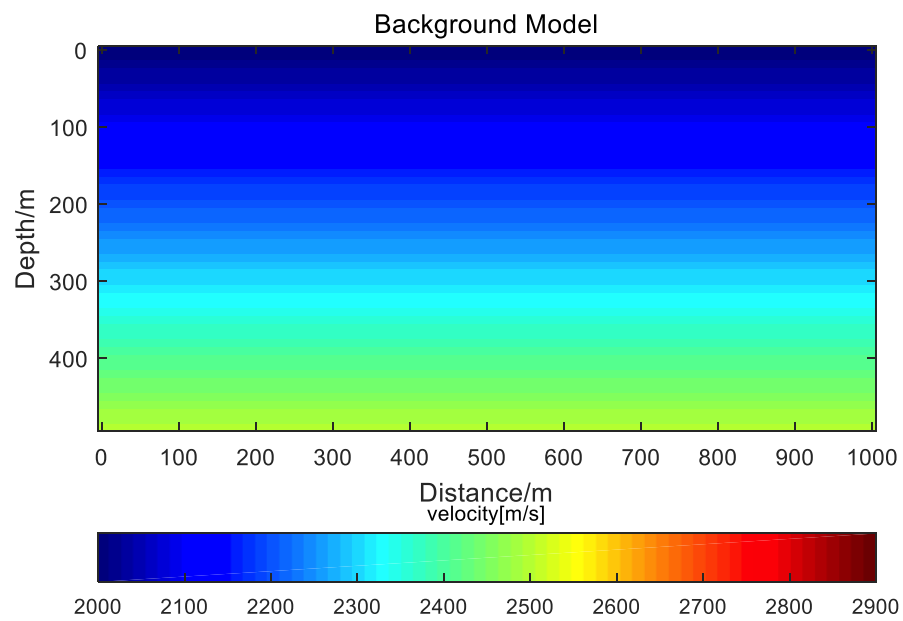
(b)

Fig. 4. (a) True layer velocity model and (b) initial/background model in the inversion.

Fig. 5a shows the inversion results using the CG method. Fig. 5b shows the inversion results obtained using the SMHCG method. Fig. 5c shows the longitudinal curves obtained from the CG and SMHCG methods at x = 500 m. Fig. 6 shows the comparison of the convergence curves for the 17 Hz of cost function at single frequency.
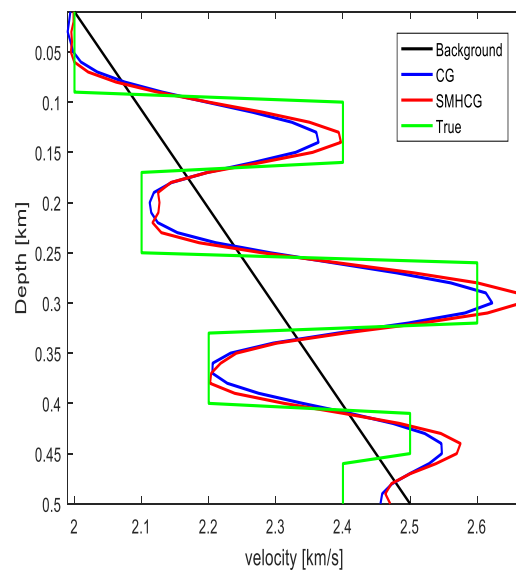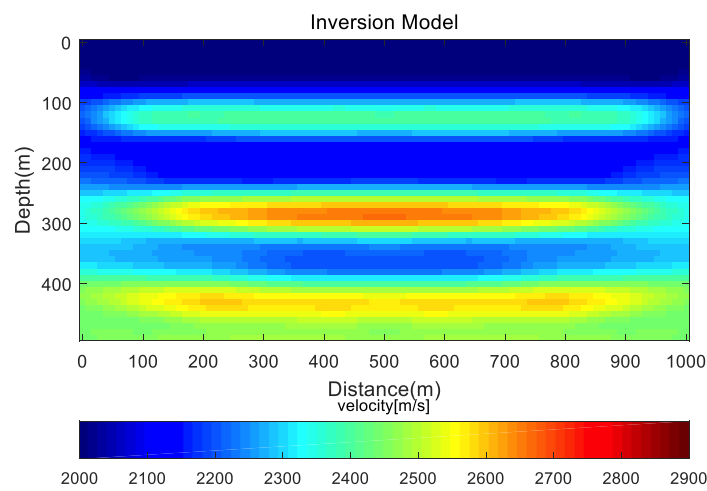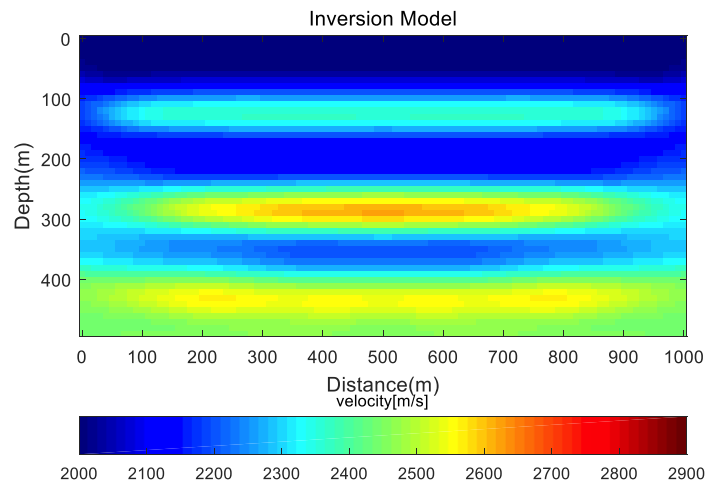
(a)

(b)

(c)

Fig. 5. (a) CG method inversion results and (b) SMHCG method inversion results and (c) longitudinal curve comparison at x = 500 m.

From the longitudinal curves retrieved from the CG and SMHCG methods in Fig. 5c, it can be seen that the SMHCG characterizes the location of velocity abrupt changes more accurately than the CG method for the same number of iterations. The L2 norm of the SMHCG inversion model and the true model residual is 6447, and the CG inversion model and the true model residual L2 norm is 7037. It can be seen from Fig. 6 that SMHCG converges faster than CG method. With the same accuracy, the SMHCG method requires fewer iterations and reduces the amount of computation.
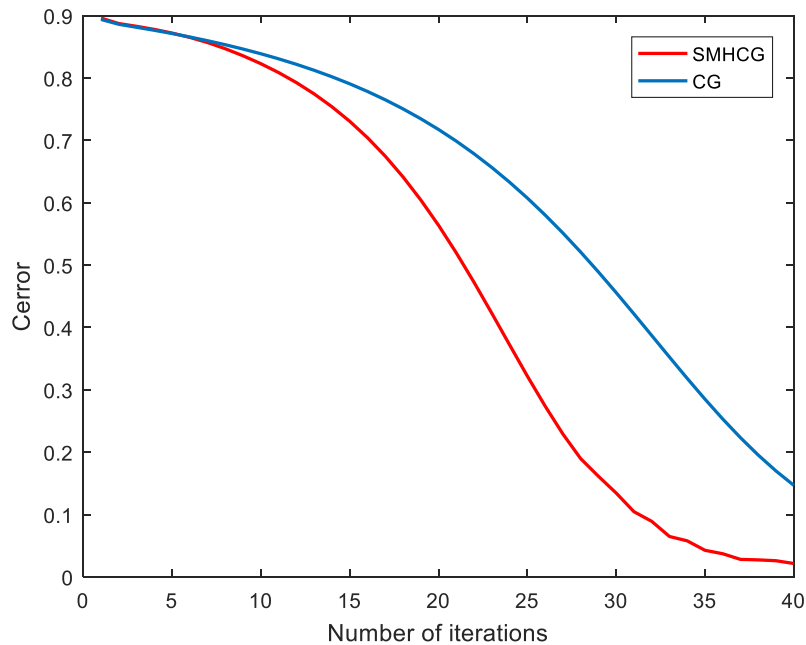
Fig. 6. CG (blue) and SMHCG (red) method 17 Hz inversion convergence curve.

Marmousi model

The Marmousi model is the standard model to validate the inversion result, so we use the two-dimensional Marmousi model to validate the method. The true Marmousi model is shown in Fig. 7a. The velocity varies from 1500 m/s to 5500 m/s. The model is 9200 m × 4000 m and the spatial grid spacing $\Delta x = \Delta z = 25m$. The acquisition system consists of 47 explosive sources and 369 receivers located at surface z = 0 m. Each shot sets 369 receivers, and detector spacing of 25 m, shot spacing of 200 m. The background model is obtained by two-dimensional mean filtering (25*25) of the true model shown in Fig. 7b. Considering the results of inversion and selection criteria of frequency we selected 9 frequencies (2, 3, 4, 5, 6, 8, 10, 12, 16 Hz) (Sirgue et al., 2004) for inversion with 120 iterations per frequency. When the number of iteration per frequency is 120, the SMHCG algorithm for CSI is converged in Marmousi model, so we used 120 iterations per frequency to verify the convergence of CG algorithm for CSI. Memory M = 7, weight factor $\lambda = 1.2$.
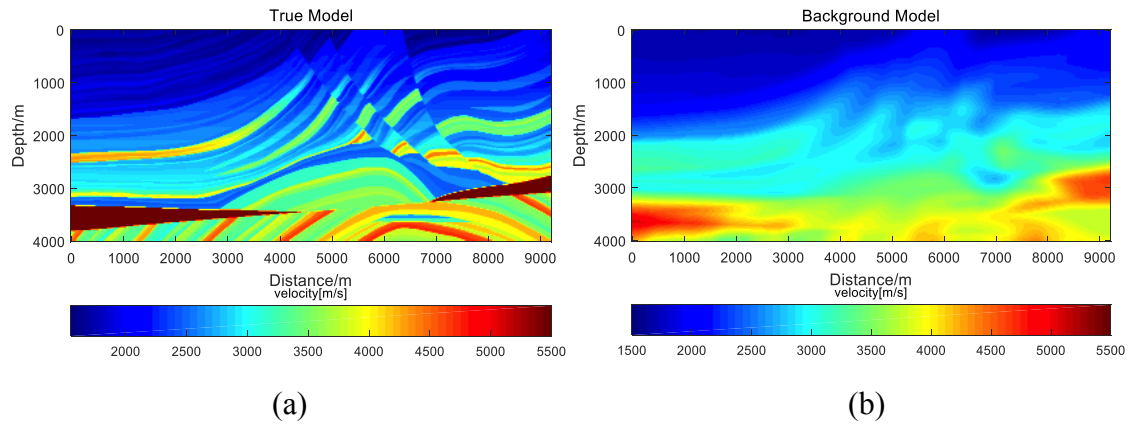
Fig. 7. (a) True Marmousi velocity model and (b) initial/background model.

Figs. 8(1a-9a) show the inversion results of 9 frequencies by the CG method, Figs. 8(1b-9b) show the inversion results of 9 frequencies by the SMHCG method. As the number of inversion frequencies increases, the inversion results become better and better, the inversion results of SMHCG are superior to CG. The inversion results in high frequency end mainly improves the details of the model, and the final inversion result by SMHCG method is more accurate. The L2 norm residuals between the real model and the final inversion results by the CG and SMHCG are 54847 and 49091. It can be seen that the SMHCG method has better results than the CG method.

(3a)

(3b)

(4a)

(4b)

(5a)

(5b)

(6a)

(6b)

(7a)   (7b)

(8a)   (8b)

(9a)   (9b)
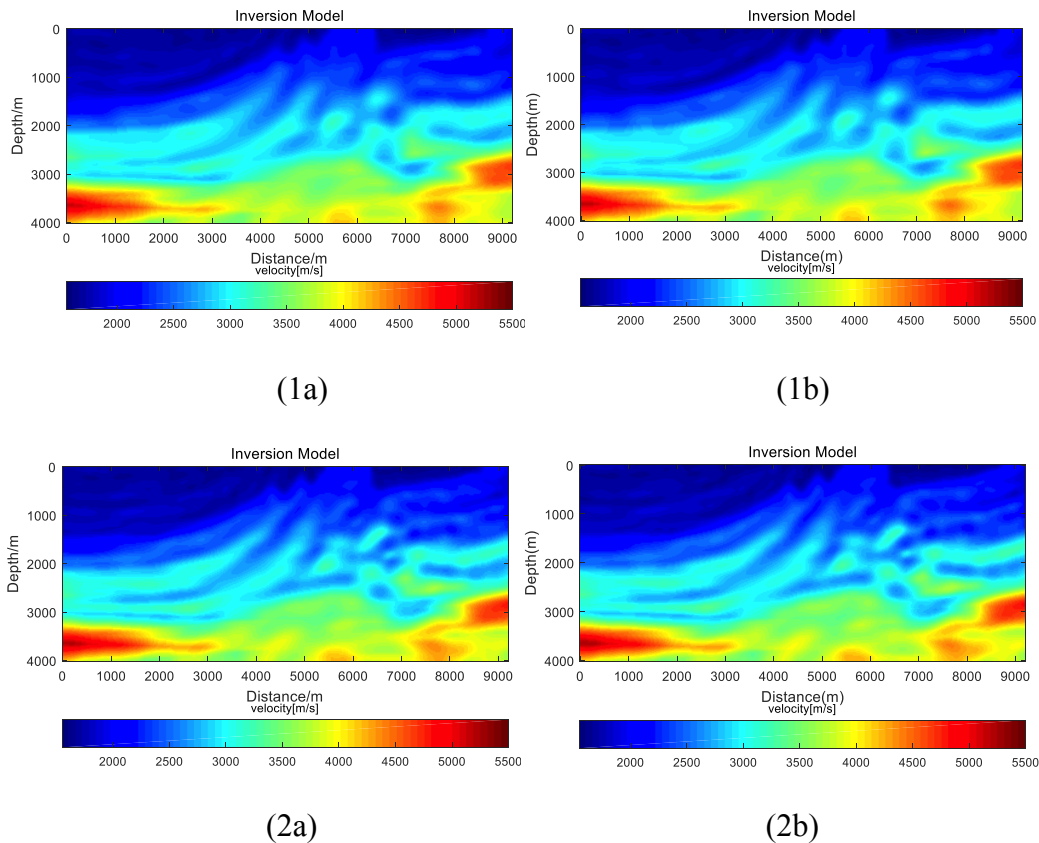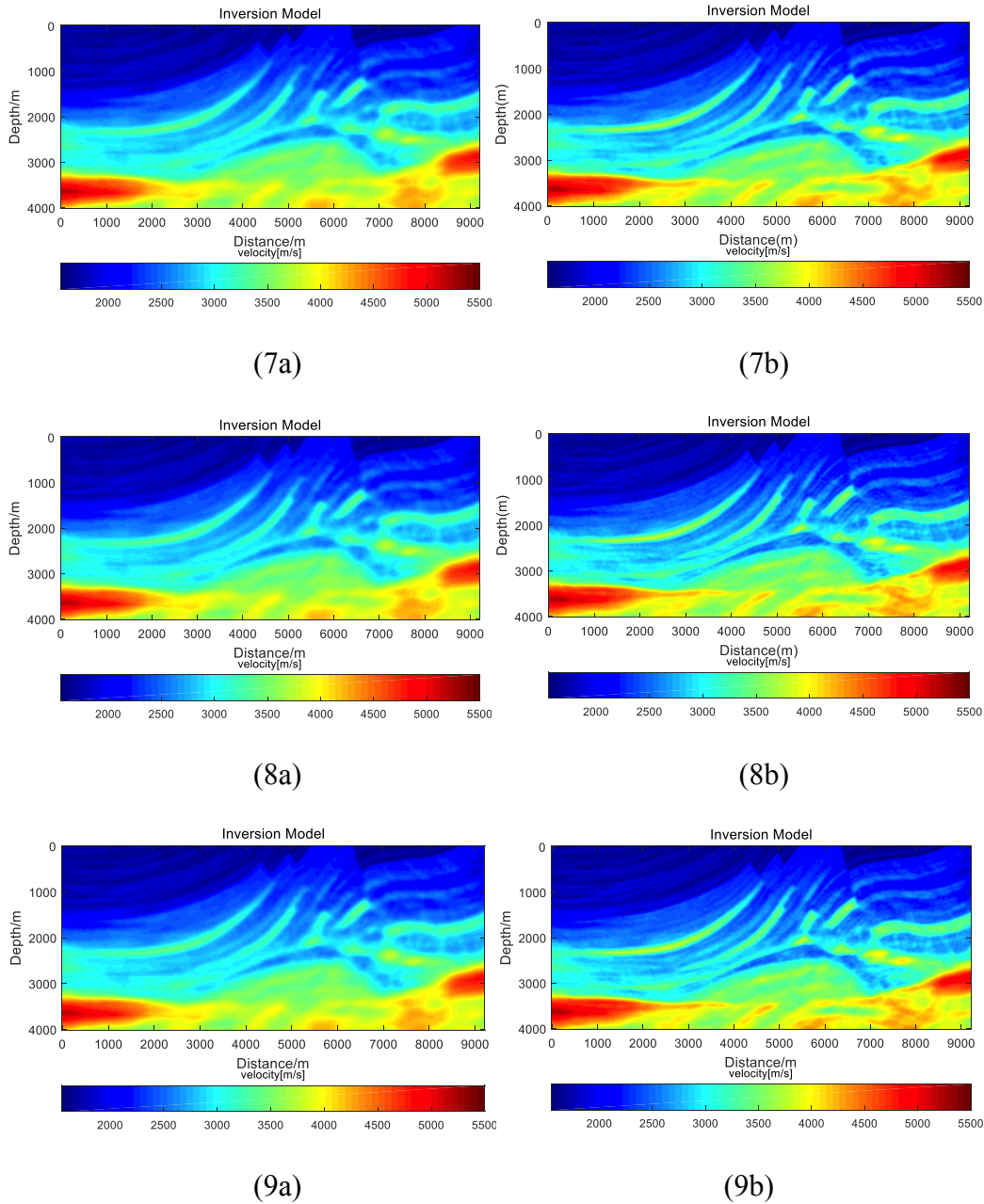
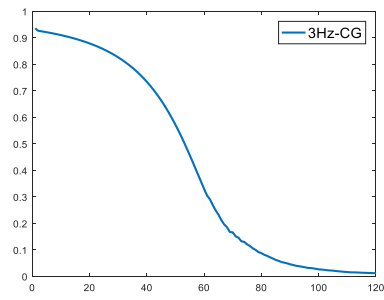Fig. 8. Figs. 1a-9a show the inversion results of 9 frequencies by CG method: (1a) 2Hz, (2a) 3Hz, (3a) 4Hz, (4a) 5Hz, (5a) 6Hz, (6a) 8Hz, (7a) 10Hz, (8a) 12Hz, (9a) 16Hz. Figs. 1b-9b show the inversion results of 9 frequencies by SMHCG method: (1b) 2Hz, (2b) 3Hz, (3b) 4Hz, (4b) 5Hz, (5b) 6Hz, (6b) 8Hz, (7b) 10Hz, (8b) 12Hz, (9b) 16Hz.

Figs. 9(1a-9a) show the cost function C convergence curves of 9 frequencies by CG, Figs. 9(1b-9b) show the cost function convergence curves of 9 frequencies by SMHCG. It can be seen that the SMHCG method has a faster convergence rate. When the iteration time is 120, the SMHCG optimization method has converged but the CG method has not converged.
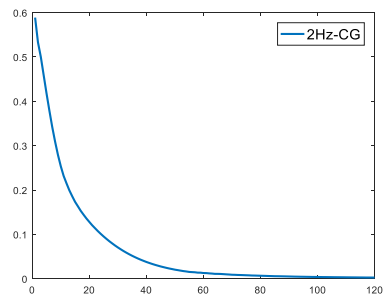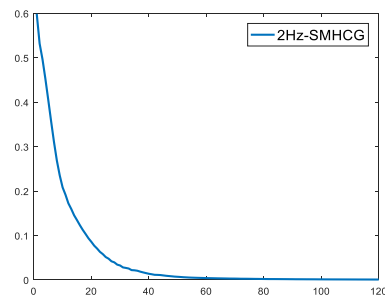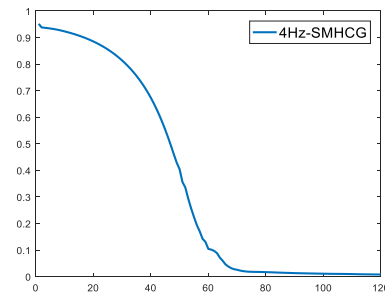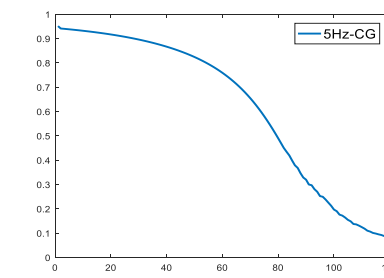
(1a)   (1b)

(2a)   (2b)

(3a)   (3b)
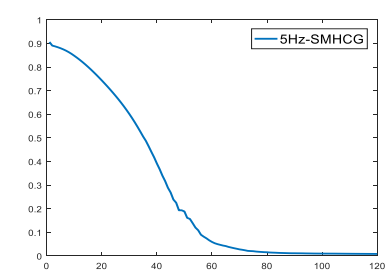
(4a)   (4b)

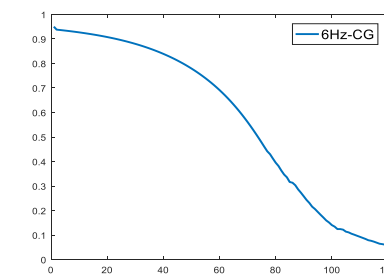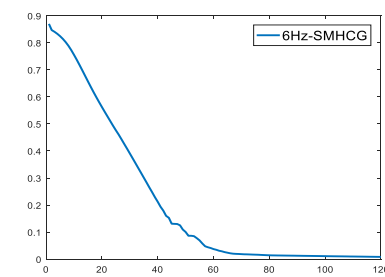(5a)   (5b)
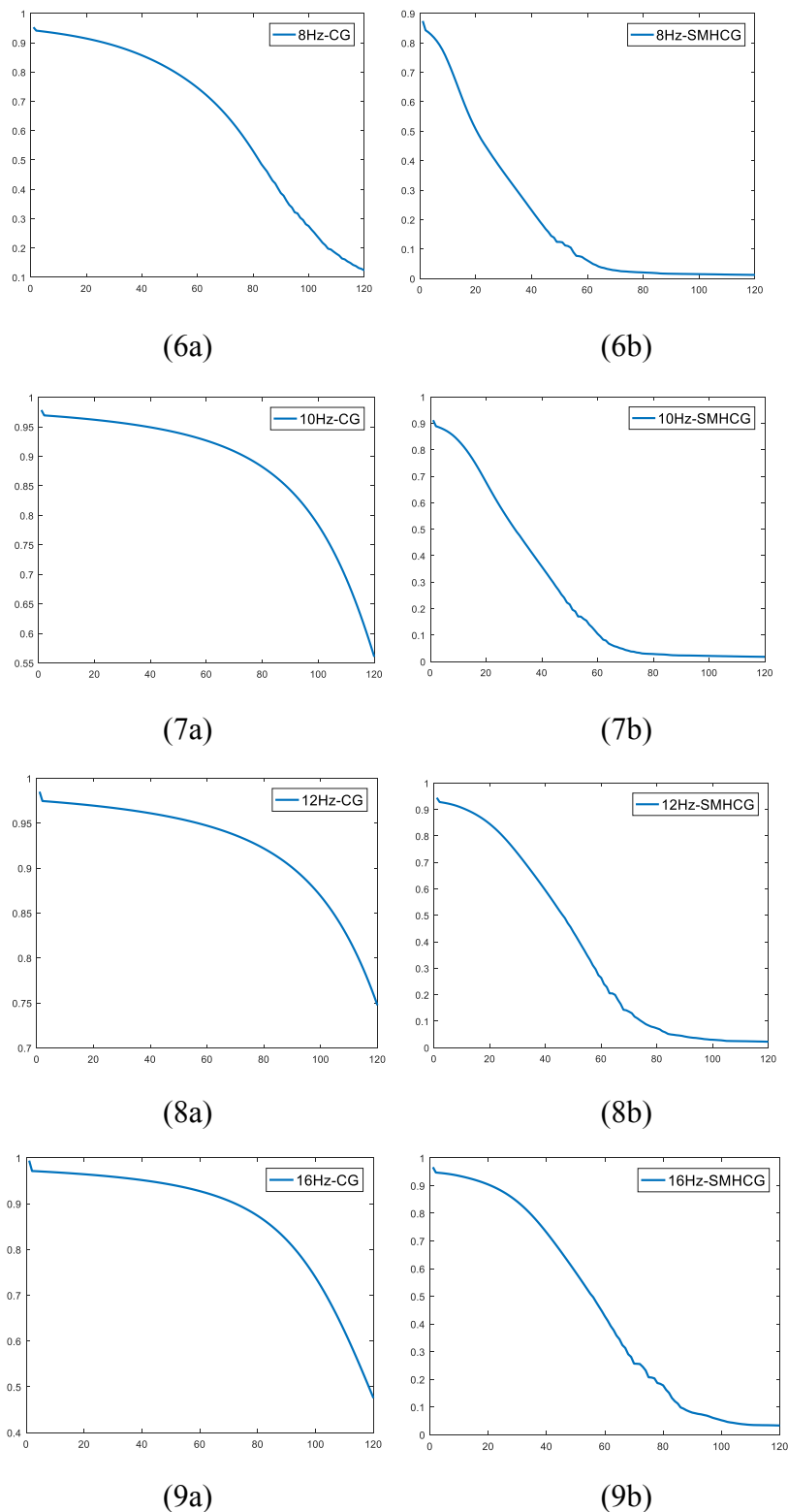
(6a)

(6b)

(7a)

(7b)

(8a)

(8b)

(9a)
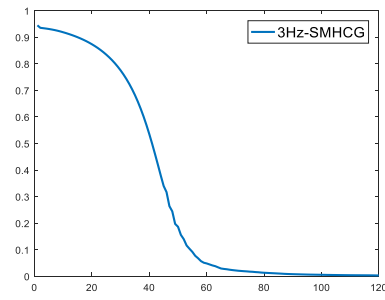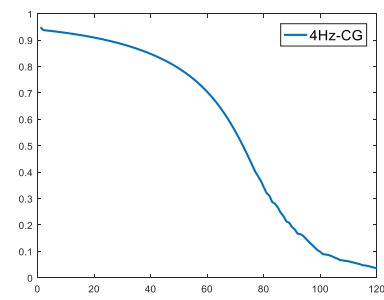
(9b)

Fig. 9. Figs.1a-9a show the convergence curves of 9 frequencies by CG method: (1a) 2Hz, (2a) 3Hz, (3a) 4Hz, (4a) 5Hz, (5a) 6Hz, (6a) 8Hz, (7a) 10Hz, (8a) 12Hz, (9a) 16Hz. Figs.1b-9b show the convergence curves of 9 frequencies by SMHCG method: (1b) 2Hz, (2b) 3Hz, (3b) 4Hz, (4b) 5Hz, (5b) 6Hz, (6b) 8Hz, (7b) 10Hz, (8b) 12Hz, (9b) 16Hz.

Figs. 10a and 10b are longitudinal curves by the CG method and SMHCG method at x = 4000 m and 5000 m. It can be seen that the SMHCG method is better than the CG method in the inversion results.
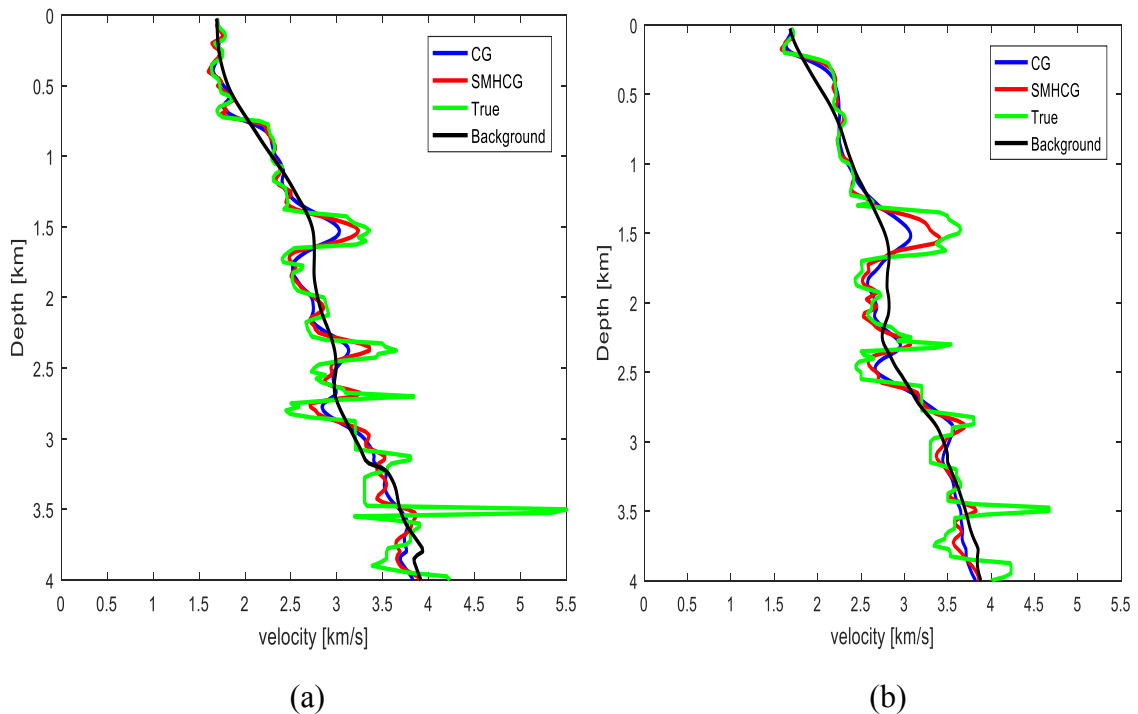

(a)   (b)

Fig. 10. (a) Longitudinal curve at x = 4000 m and (b) Longitudinal curve at x = 5000 m.

Test to calculate efficiency

In order to verify the effectiveness of this method, we conducted an efficient quantitative test of the Marmousi model. Define data residuals as follows

$$ERR_d = \frac{\left\| d_{obs,j}^{sct} - d_{cal,j}^{sct} \right\|_D^2}{\left\| d_{obs,j}^{sct} \right\|_D^2} \quad , \tag{30}$$

where $d_{cal,j}^{sct}$ is the forward scattering wave field. Nine frequencies (2, 3, 4, 5, 6, 8, 10, 12, 16 Hz) are chosen for inversion, and the termination condition for each frequency iteration is: $ERR_d \le 0.005$. Because SMHCG adds only additive operations compared to CG methods, the SMHCG and CG methods can be considered equal time-consuming for a single iteration. So the inversion efficiency of SMHCG and CG methods is only related to the number of iterations.

Figs. 11 and 12 show the velocity model and the longitudinal velocity curve of the Marmousi model retrieved by the CG and SMHCG methods. It can be seen from the figure that the results of the two methods are basically the same, but the CG method needs to iterate 1363 times and the SMHCG method only needs 861 times. The SMHCG method is 36% more efficient than the CG method. Fig. 13 shows the comparison of the convergence curves of the two methods when the frequency is 8 Hz. It can be seen that the SMHCG method converges to the iterative termination accuracy faster than CG method.
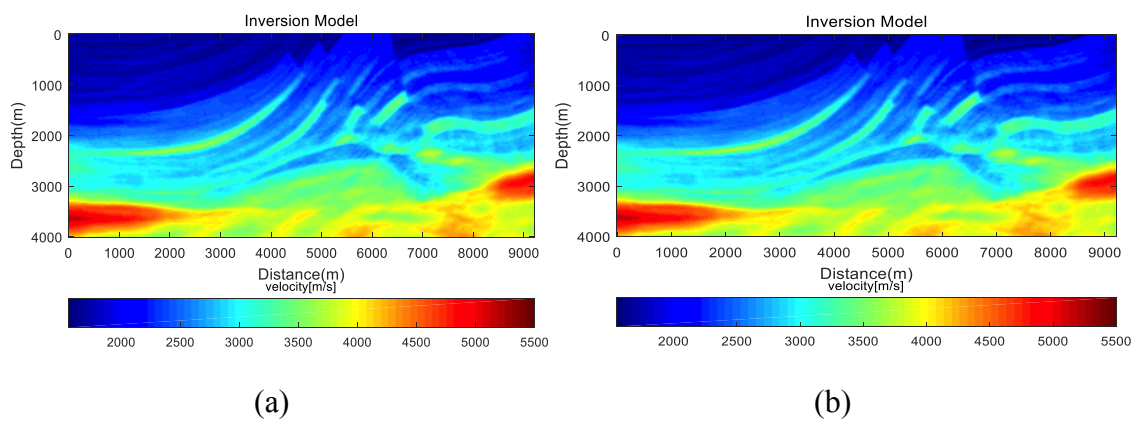

(a)   (b)

Fig. 11. (a) CG method inversion result and (b) SMHCG method inversion result.

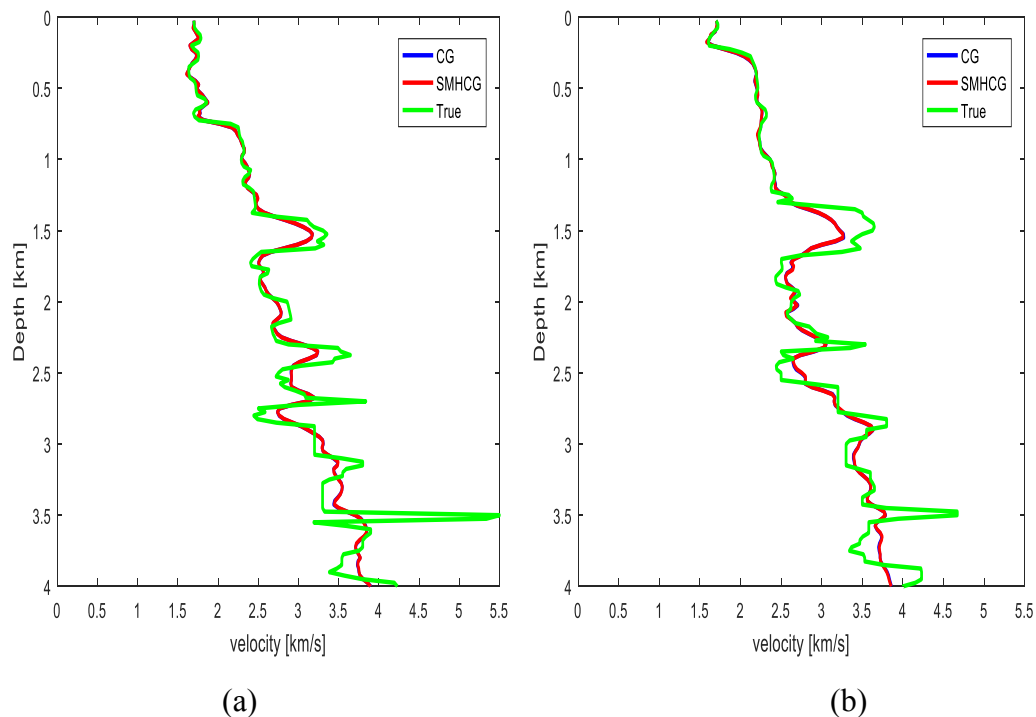

(a)   (b)

Fig. 12. (a) Longitudinal curve at x = 4000 m and (b) Longitudinal curve at x = 5000 m.
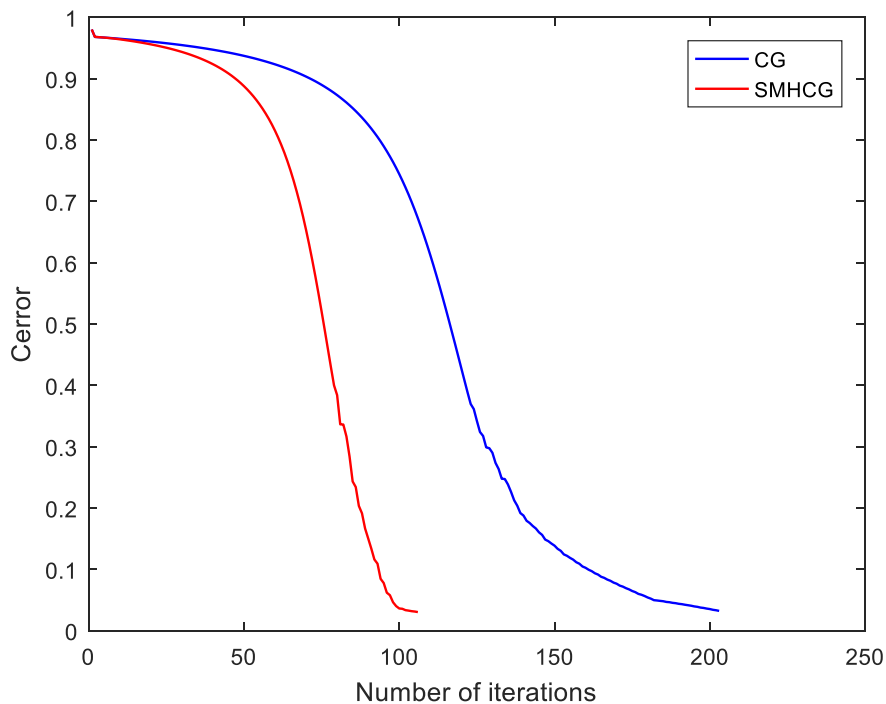
Fig. 13. CG (blue) and SMHCG (red) method 8 Hz inversion convergence curve of the objective function.

DISCUSSION

Although CSI can reduce computational cost and SMHCG algorithm can accelerate the convergence of the target function, both inversion results can not define the high velocity zone (at 3.5 km). The Marmousi model is a very complex model in exploration geophysics. The high velocity zone is a difficult part of inversion in the Marmousi model. And other inversion methods also have such problems. Besides, there are three problems: first, CSI is based on the hypothesis of weak scattering, there should not be much disparity between inversion model and background model; second, as the high velocity zone is located at the boundary of the model, the fold number is insufficient, and the effective information obtained is less; last, there are nine frequencies used for inversion, it is impossible to reconstruct the overlying strata accurately, which will affect the inversion of the high velocity zone.

CONCLUSIONS

The FDCSI is a method to solve the inverse scattering problem of the wave equation. In the inversion process, the background model does not change, so we only need to construct forward matrix and LU decomposition once. Therefore, the inversion efficiency is greatly improved. The conventional conjugate gradient method has the problem of slow convergence and time-consuming in solving the contrast source and contrast.

Based on the FDCSI method of acoustic equation, this paper introduces a super-memory hybrid conjugate gradient optimization method, which accelerates the convergence speed of the method without increasing the computational complexity, reduces the number of iterations, saves the computation time. In this paper, the SMHCG method is used to verify the Marmousi model, and the efficiency is improved by 36%, which is in favor of the inversion of 3D data. In this paper, we only study the contrast source inversion of the acoustic wave equation with constant medium density. Contrast source inversion of elastic media with complex media, variable density and variable Q value need to be studied. This method can be extended to variable density, multi-parameter viscoelastic medium contrast source inversion, so as to more truly reflect the underground media situation.

ACKNOWLEDGMENTS

REFERENCES

Abubakar, A., Hu, W., van den Berg, P.M. and Habashy, T.M., 2008. A finite-difference contrast source inversion method. Inverse Probl., 24: 065004-065020.

Abubakar, A., Hu, W., Habashy, T.M. and van den Berg, P.M., 2009. Application of the finite-difference contrast-source inversion algorithm to seismic full-waveform data. Geophysics, 74(6): WCC47-WCC58.

Abubakar, A., Pan, G.D., Li, M. and Zhang, L., 2011. Three-dimensional seismic full-waveform inversion using the finite-difference contrast source inversion method. Geophys. Prosp., 59: 874-888.

Berenger, J.P., 1994. A perfectly matched layer for the absorption of electromagnetic waves. Academic Press Professional, Inc.

van den Berg, P.M. and Kleinman, R.E., 1997 A contrast source inversion method. Inverse Probl., 13: 1607-1620.

van den Berg, P.M., van Broekhoven, A.L. and Abubakar, A., 1999. Extended contrast source inversion. Inverse Probl., 15: 1325-1344.

Brossier, R., Operto, S. and Virieux, J., 2009. Seismic imaging of complex onshore structures by 2D elastic frequency-domain full-waveform inversion. Geophysics, 74(6): WCC105-WCC118.

Chi, B., Dong, L. and Liu, Y., 2014. Full waveform inversion method using envelope objective function without low frequency data. J. Appl. Geophys., 109: 36-46.

Choi, Y., Shin, C., Min, D.J. and Ha, T., 2005. Efficient calculation of the steepest descent direction for source-independent seismic waveform inversion: An amplitude approach. J. Computat. Phys., 208: 455-468.

Davis, T.A. and Duff, I.S., 2006. An unsymmetric-pattern multifrontal method for sparse LU factorization. Soc. Industr. Appl. Mathemat., 18: 140-158.

van Dongen, K.W. and Wright, W.M., 2007. A full vectorial contrast source inversion scheme for three-dimensional acoustic imaging of both compressibility and density profiles. J. Acoust. Soc. Am., 121: 1538.

Habashy, T.M., Oristaglio, M.L. and Hoop, A.T.D., 2016. Simultaneous nonlinear reconstruction of two-dimensional permittivity and conductivity. Radio Sci., 29: 1101-1118.

Han, B., He, Q.L., Chen, Y. and Dou, Y.X., 2014. Seismic waveform inversion using the finite-difference contrast source inversion method. J. Appl. Mathemat., 10: 1-11.

He, Q.L., Han, B., Chen, Y. and Li, Y., 2016. Application of the finite-difference contrast source inversion method to multiparameter reconstruction using seismic full-waveform data. J. Appl. Geophys., 124: 4-16.

Hu, Y., Han, L.G., Zhang, P., Bai, L. and Zhang, T.Z., 2016. Hybrid super memory gradient method ull waveform inversion. Extended Abstr., 78th EAGE Conf., Vienna.

Jo, C.H., Shin, C.S. and Suh, J.H., 1996. An optimal 9-point, finite-difference, frequency-space, 2-D scalar wave extrapolator. Geophysics, 61: 529-537.

Kamei, R., Pratt, R.G. and Tsuji, T., 2015. Misfit functionals in Laplace-Fourier domain waveform inversion, with application to wide-angle ocean bottom seismograph data. Geophys. Prosp., 62: 1054-1074.

Kim, W.K. and Min, D.J., 2014. A new parameterization for frequency-domain elastic full waveform inversion for VTI media. J. Appl. Geophys., 109: 88-110.

Lysmer, J. and Drake, L.A., 1972. A Finite Element Method for Seismology. Methods Computat. Phys. Advan. Res. Applicat., 11: 181-216.

Métivier, L., Brossier, R., Virieux, J. and Operto, S., 2015. Full waveform inversion and the Truncated Newton Method: quantitative imaging of complex subsurface structures. Geophys. Prosp., 62: 1353-1375.

Ou, Y. and Liu, Y., 2013. A nonmonotone supermemory gradient algorithm for unconstrained optimization. J. Appl. Mathemat. Comput., 46: 215-235.

Ou, Y. and Liu, Y., 2017. Supermemory gradient methods for monotone nonlinear equations with convex constraints. Computat. Appl. Mathemat., 36: 259-279.

Pelekanos, G., Abubakar, A. and van den Berg, P.M., 2003. Contrast source inversion methods in elastodynamics. J. Acoust. Soc. Am., 114: 2825-2834.

Pratt, R.G. and Worthington, M.H., 1990. Inverse theory applied to multi-source cross-hole tomography: Part 1. Acoustic wave-equation method. Geophys. Prosp., 38: 287-310.

Pratt, R.G., 1999. Seismic waveform inversion in the frequency domain, Part 1: theory and verification in a physical scale model. Geophysics, 64: 888-901.

Pratt, R.G., Shin, C. and Hick, G.J., 1998. Gauss-Newton and full Newton methods in frequency space seismic waveform inversion. Geophys. J. Internat., 133: 341-362.

Pratt, R.G. and Worthington, M.H., 1990. Inverse theory applied to multi-source cross-hole tomography Part1: acoustic wave equation method: Geophysical Prospecting, 38(3), 287-310.

Shi, Z.J. and Shen, J., 2005. A new super-memory gradient method with curve search rule. Appl. Mathemat. Computat., 170: 1-16.

Shin, C., 1995. Sponge boundary condition for frequency-domain modeling. Geophysics, 60: 1870-1874.

Sirgue, L. and Pratt, R.G., 2004. Efficient waveform inversion and imaging: A strategy for selecting temporal frequencies. Geophysics, 69: 231-248.

Tarantola, A., 1986. A strategy for nonlinear elastic inversion of seismic reflection data. Geophysics, 51: 1893-1903.

Ugeun, J., Min, D. and Shin, C.S., 2010. Comparison of scaling methods for waveform inversion. Geophys. Prosp., 57: 49-59.

Wang, S.D., Wu, R.S. and Liu, Y.F., 2016. The contrast source inversion for reflection seismic data. Extended Abstr., 78th EAGE Conf., Vienna.

Weng, C.C. and Weedon, W.H., 1994. A 3D perfectly matched medium from modified Maxwell's equations with stretched coordinates. Microw. Optic. Technol. Lett., 73: 599-604.